Journal Pre-proof

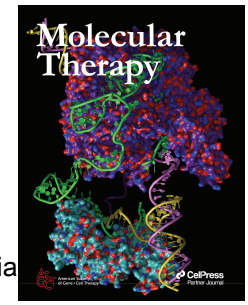

Therapeutic AASS inhibition by AAV-miRNA rescues glutaric aciduria type I severe phenotype in mice

Eulàlia Segur-Bailach, Anna Mateu-Bosch, Xavier Bofill-De Ros, Marta Parés, Patricia da Silva Buttkus, Birgit Rathkolb, Valérie Gailus-Durner, Martin Hrabě de Angelis, Pedram Moeini, Gloria Gonzalez-Aseguinolaza, Frederic Tort, Antonia Ribes, Clara D.M. van Karnebeek, Judit García-Villoria, Cristina Fillat

PII: S1525-0016(25)00558-1

DOI: https://doi.org/10.1016/j.ymthe.2025.07.022

Reference: YMTHE 7027

To appear in: *Molecular Therapy*

Received Date: 8 January 2025

Accepted Date: 13 July 2025

Please cite this article as: Segur-Bailach E, Mateu-Bosch A, Bofill-De Ros X, Parés M, da Silva Buttkus P, Rathkolb B, Gailus-Durner V, Hrabě de Angelis M, Moeini P, Gonzalez-Aseguinolaza G, Tort F, Ribes A, van Karnebeek CDM, García-Villoria J, Fillat C, Therapeutic AASS inhibition by AAV-miRNA rescues glutaric aciduria type I severe phenotype in mice, *Molecular Therapy* (2025), doi: https://doi.org/10.1016/j.ymthe.2025.07.022.

This is a PDF file of an article that has undergone enhancements after acceptance, such as the addition of a cover page and metadata, and formatting for readability, but it is not yet the definitive version of record. This version will undergo additional copyediting, typesetting and review before it is published in its final form, but we are providing this version to give early visibility of the article. Please note that, during the production process, errors may be discovered which could affect the content, and all legal disclaimers that apply to the journal pertain.

© 2025 The Author(s). Published by Elsevier Inc. on behalf of The American Society of Gene and Cell Therapy.

Journal Pre-proof

AAV9_miR_AASS Subtrate reduction therapy for GA1

Untreated GA1 Severe Phenotype

GA
3-OHGA

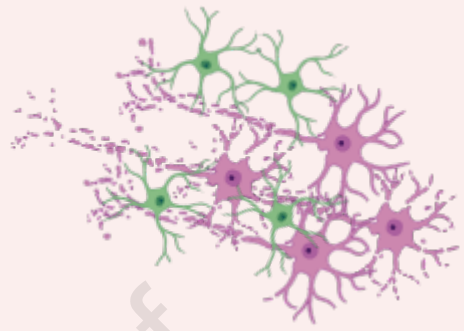

Birth
Weaning

Treatment

HLD exposition

Lysine
AASS
mRNA degradation and translational represion
Glutaryl-CoA
GA
3-OHGA
GCDH
Acetyl-CoA
RISC
mature miRNA
pre-miRNA
pri-miRNA

AAV9_miR_AASS Severe Phenotype Amelioration

GA
3-OHGA

Prevents toxic metabolites

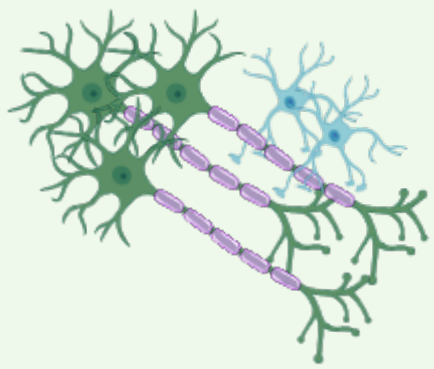

Prevents neuropathologic alterations

Improves survival

Journal Pre-proof

Therapeutic AASS inhibition by AAV-miRNA rescues glutaric aciduria type I severe phenotype in mice

Eulàlia Segur-Bailach[1,2], Anna Mateu-Bosch[1], Xavier Bofill-De Ros[3], Marta Parés[1], Patricia da Silva Buttkus[4], Birgit Rathkolb[4,10,11], Valérie Gailus-Durner[4], Martin Hrabě de Angelis[4,9,10], Pedram Moeini[5], Gloria Gonzalez-Aseguinolaza[5], Frederic Tort[1,2,6], Antonia Ribes[1,2,6], Clara D M van Karnebeek[7], Judit García-Villoria[1,2,6], and Cristina Fillat [1,2,8*]

[1] Institut d'Investigacions Biomèdiques August Pi i Sunyer (IDIBAPS), 08036 Barcelona, Spain.
[2] Centro de Investigación Biomédica en Red de Enfermedades Raras (CIBERER), 08036 Barcelona, Spain.
[3] Department of Molecular Biology and Genetics, Aarhus University, Aarhus, Denmark.
[4] Institute of Experimental Genetics, German Mouse Clinic, Helmholtz Zentrum München, 85764 Neuherberg, Germany.
[5] DNA & RNA Medicine Division, Gene Therapy for Rare Diseases Department, Center for Applied Medical Research (CIMA), University of Navarra, IdisNA, Pamplona, Spain.
[6] Secció d'Errors Congènits del Metabolisme-IBC, Servei de Bioquímica i Genètica Molecular, Hospital Clínic de Barcelona, 08028 Barcelona, Spain.
[7] Departments of Pediatrics and Human Genetics, Emma Center for Personalized Medicine, Amsterdam Gastro-Enterology Endocrinology Metabolism, Amsterdam University Medical Centers, Amsterdam, The Netherlands.
[8] Facultat de Medicina i Ciències de la Salut. Universitat de Barcelona, 08036 Barcelona, Spain.
[9]Chair of Experimental Genetics, TUM School of Life Sciences, Technische Universität München, 85354 Freising, Germany
[10]German Center for Diabetes Research (DZD), 85764 Neuherberg, Germany
[11]Institute of Molecular Animal Breeding and Biotechnology, Genecenter, Ludwig-Maxumilians- Universitaet Muenchen, 81377 Munich, Germany

* Corresponding author. E-mail: cfillat@recerca.clinic.cat Institut d'Investigacions Biomèdiques August Pi i Sunyer (IDIBAPS), 08036 Barcelona, Spain

Journal Pre-proof

Journal Pre-proof

Abstract

Glutaric aciduria type I (GA1) is an inherited disorder caused by the enzymatic defect of glutaryl-CoA dehydrogenase in the lysine degradation pathway, characterized by the accumulation of toxic metabolites in the central nervous system. We reasoned that substrate reduction therapy targeting the alpha-Aminoadipic Semialdehyde Synthase (AASS), the first enzyme in the catabolism of lysine, could provide an attractive therapeutic alternative. We explored to reduce the expression of AASS by an artificial microRNA with AASS target sequences embedded in a miR-16 backbone (miR_AASS). We analyzed several delivery routes and AAV serotypes and evaluated the therapeutic efficacy of a systemic neonatal delivery of AAV9_miR_AASS in the *Gcdh-/-* mouse model of GA1. We detected dose-dependent miR-AASS expression and AASS inhibition in liver and striatum, the main tissues affected in GA1. Treatment with AAV9_miR_AASS in lysine overload challenged mice reduced the accumulation of neurotoxic metabolites, up to six months post-treatment in the striatum, prevented the neuropathological alterations and improved mouse survival. Our results show that AAV9_miR_AASS supports AASS-lowering as a potential gene therapy strategy for GA1.

Journal Pre-proof

Journal Pre-proof

INTRODUCTION

Glutaric aciduria type 1 (GA1; MIM: 231670) is an autosomal recessive inborn error of metabolism caused by inherited deficiency of glutaryl-CoA dehydrogenase (GCDH), an enzyme involved in the catabolism of lysine, tryptophan and hydroxylysine. GA1 was first discovered in 1975 [1] and has a variable prevalence ranging from 1:100.000 in the general population to 1:250 newborns in high-risk populations. [2,3] Pathogenic variants in GCDH cause the defective oxidation and posterior decarboxilation of glutaryl-CoA in the lysine degradation pathway, resulting in disease-specific metabolites accumulation such as glutaric (GA) and 3-hydroxyglutaric (3-OHGA) acid in body fluids and tissues. These intermediates accumulate mainly in the central nervous system (CNS), due to the lack of cerebrovascular transporters and the low permeability of the blood brain barrier (BBB). Increased concentration of neurotoxic metabolites triggers the clinical features of GA1, characterized by acute encephalopathic crises which lead to permanent bilateral striatal injury.[4,5] Most untreated patients develop the acute encephalopathic crises between the ages of 3 and 36 months, precipitated by catabolic events such as intercurrent febrile illness or prolonged fasting caused by infections or surgical procedures. After these episodes, individuals develop dystonia, complex movement disorders and spasticity, with severe neurological irreversible damage. [3,6,7] The life expectancy of affected individuals varies significantly, while some may reach adulthood, about half of the affected children do not survive their first decade of life due to an acute episode. GA1 is currently early diagnosed via newborn screening in some countries and controlled by restricting lysine intake, carnitine supplementation, and emergency treatment. [8] Although dietetic lysine restriction is considered safe and effective, one-third of the patients still experience striatal damage despite early diagnosis and treatment. [2,9]

Since lysine is an essential amino acid it can not be reduced below the minimal daily requirements, limiting the therapeutical range of this diet. Substrate reduction therapies

for inborn errors of metabolism arises as a potential therapeutic strategy to decrease the levels of toxic metabolites by inhibiting an enzyme upstream of the defective enzyme. In fact, the inhibition of the first enzyme in the lysine catabolic pathway, the alpha-aminoadipic semialdehyde synthase (AASS) enzyme has been suggested as a strategy for the treatment of GA1. [10] Interestingly, deficiency in AASS, leads to hyperlysinemia (MIM: 238700) considered a benign entity without apparent clinical consequences. Therefore, inhibition of this specific enzyme would be a safe target in humans. [10–12]

In this study, we used *Gcdh*$^{-/-}$ mice as a model of GA1, with the aim of developing a gene therapy approach to inhibit AASS based on an artificial microRNA (miRNA) targeting *Aass* transcript delivered by an adeno-associated virus 9 (AAV9) or AAV9P31. We demonstrate that a single neonatal intravenous administration of AAV_miR_AASS in *Gcdh*$^{-/-}$ mice prevents the accumulation of GA and 3-OHGA, mitigates striatal damage, and rescues the lethal phenotype in mice fed in a High Lysine Diet (HLD). We suggest that a substrate reduction therapy that limits the pathophysiological manifestations of GA1 neurotoxic metabolites accumulation may be further explored as a treatment option for GA1, with potential application to other inborn errors of lysine metabolism.

Journal Pre-proof

RESULTS

Artificial miR_AASS sequences efficiently inhibit AASS from a pri-miR-16 backbone

Four DNA sequences with 100% homology in the seed sequence between the orthologous mouse *Aass* and human AASS genes were selected to design the artificial miRNAs (miR_AASS) (**Figure S1A, S1C**). These sequences also fit the criteria of: i) targeting the structural domains of the protein, ii) exclusively binding to the target sequence and iii) improving miRNA thermodynamic stability for optimal miRNA biogenesis. [13,14] Selected sequences were embedded in the pri-miR16 scaffold under the control of the eukaryotic CAG promoter (**Figure S1B**). To evaluate the knockdown efficiency of the different sequences, HEK293 cells were cotransfected with the miR_AASS constructs (**Figure S1B**) and the pLuc_*AASS* or the pLuc_*Aass* reporter cassettes. The reporter constructs beared a partial *AASS* or *Aass* cDNA containing the target sequences fused to the Renilla Luciferase, in a backbone that contained Firefly Luc, used to correct for transfection efficiency (**Figure S1D**). The four sequences triggered human Luc_AASS inhibition in a range of 40-60%. Sequences 3 and 4 (miR_3, miR_4) were the most effective leading to 90% and 75% inhibition, respectively, of mouse Luc_*Aass* and were selected for future studies (**Figure S1E**). The higher efficiency towards the mouse sequences could be related to the fact that the 22 nucleotide sequences, with 100% homology in the seed sequence (murine and human), displayed perfect complementarity for the murine sequence and variable level of mismatches for the human sequence (**Figure S1C**). Despite single nucleotide mismatched are in general well tolerated for silencing efficacy, close to perfect complementarities are considered the best. [15,17] The general higher activity of seq 3 and 4 on both transcripts suggest higher accessibility to this region, since sequences 1 and 2 are located close to the 3' end of the transcript, whereas sequences 3 and 4 cluster

together and far from the 3' end (**Figure S1A**). In fact, differences in the sequence surrounding the target sites have been shown to modulate the efficacy. [19]

To further assess the inhibitory capacity of miR_3 and miR_4 on human and mouse endogenous AASS, we generated stable cells lines expressing the indicated sequences in the murine NIH3T3 and the human SH-SY5Y cells. We observed similar inhibition of both sequences in human AASS expression both at protein and RNA levels (**Figures 1A and 1B**). However, miR_4 was more efficient inhibiting mouse AASS (**Figures 1C and 1D**). The high silencing efficiency of miR_4 may be attributed to its target sequence being located within an exon, whereas the target site for miR_3 lies in an exon-exon junction. Consequently, miR_4 activity may occur on both pre-mRNA and mature mRNA. In this line, there are several reports describing that AGO molecules in the nucleus can effectively regulate gene expression. [21] To confirm the specificity of miR_4 sequence, we generated a miR_4sc construct bearing the same sequence 4 but in scrambled organization and obtained NIH3T3 cells expressing miR_4sc (**Figure S2A**). Western blot analysis confirmed that miR_4 but not miR_4sc downregulated AASS expression (**Figure S2B**). To assess the effect of miR_4 on the AASS activity, we conducted an enzyme assay based on the consumption of the NADPH substrate when cells were stimulated with 10 mM lysine for 72h. WT but not miR_4 expressing cells were capable of reducing NADPH consumption, indicating defective enzyme activity in miR_4 expressing cells (**Figure 1E and 1F**). Thus, the noticeable silencing effect of miR_4 and their capacity to modulate AASS activity prompted us to select miR_4 for future *in vivo* studies.

Correction of GA and 3-OHGA metabolite accumulation by inhibition of AASS through AAV vectors encoding miR_AASS

We were interested to explore the potential benefits of AASS inhibition in glutaric aciduria type I. The *Gcdh-/-* mouse with complete loss of GCDH activity is a well-characterized

155 animal model for GA1 that reproduces the biochemical alterations present in GA1
156 patients. [16] We set out to study the capacity of rescuing the biochemical alterations in the
157 mouse model through the inhibition of AASS with an AAV9 vector containing the miR_4
158 sequence (from now named AAV9_miR_AASS). Moreover, since the AAV9P31 serotype
159 has been reported to target both liver and brain in adult mice we also generated
160 AAV9P31_miR_AASS (**Figure 2A**). [18,20] Young adult *Gcdh-/-* mice 30-days old (P30) of
161 both sexes were treated with AAV9_miR_AASS or AAV9P31_miR_AASS by intravenous
162 (IV) delivery through tail vein injection (7.5 x 10^{12} vg/kg). Moreover, we also tested the
163 effects of AAV9_miR_AASS delivery after locoregional intracisternal magna
164 administration (CM) at 7.5 x 10^{12} vg/kg. *Gcdh-/-* mice receiving either vector were
165 euthanized 1-month post-treatment and the effects of RNA interference-based AASS
166 inhibition were assessed in the liver and the striatum, since these are the most affected
167 tissues in GA1 mice. Mature miR_AASS transcripts were detected in all the conditions
168 tested in liver, whereas they were not detected in the striatum of AAV9_miR_AASS
169 treated mice when administered intravenously (**Figure 2B and 2C**). However, IV
170 administration of AAV9P31_miR_AASS resulted in very high miR_AASS transcript in the
171 striatum, significantly higher than CM delivery of AAV9_miR_AASS (**Figure 2C**). A range
172 of 40% to 50% inhibition of AASS expression was observed in the liver with all the
173 strategies (**Figure 2D**). However, in the striatum the knockdown efficiency varied
174 between the three strategies, with the AAV9P31_miR_AASS knockdown showing the
175 strongest effect (**Figure 2E**). Analysis of the biochemical metabolites GA and 3-OHGA
176 confirmed increased concentrations in the liver and striatum of *Gcdh-/-* mice when
177 compared to WT animals. Treatment with AAV9_miR_AASS or AAV9P31_miR_AASS
178 reduced both GA and 3-OHGA accumulation in the liver. However, only
179 AAV9P31_miR_AASS treatment reduced metabolite content in the striatum, with
180 statistical significance for 3-OHGA, the most toxic metabolite accumulated in GA1
181 (**Figure 2F and 2G**). These results validate the intravenous administration of
182 AAV9P31_miR_*AASS* in adult GA1 mice to correct the metabolic defects in the striatum.

These promising results were in accordance with recent findings of the use of this modified serotype for the evaluation of CNS-directed therapies in mouse models. [20]

Most untreated individuals in GA1 experience acute encephalopathic crises during the first 6 years of life, what makes early therapy essential to prevent significant neurologic injury. Thus, we decided to explore whether miR_AASS therapy when delivered IV at neonatal stage (P1) could modulate the metabolite content. We decided to perform these experiments with the vector based on the AAV9 serotype since previous studies have shown that neonatal intravenous administration of AAV9 vectors is an efficient approach to deliver AAV products to the striatum. [22,23] Moreover, the translational value of the use of this serotype in human patients has already been reported for a variety of disorders. [24]

We tested two viral doses: a low dose of 7.5×10^{12} vg/kg and a high dose of 5×10^{13} vg/kg and analyzed the effects 1-month post-treatment. Mature miR_AASS transcripts were detected at the two doses in both liver and the striatum in a dose-dependent manner (**Figures 3A and 3B**). Inhibition of the AASS protein was also observed at all the doses tested, with a 70% knockdown in the striatum of mice receiving the highest dose (**Figure 3C and 3D**). Interestingly, at the highest dose both GA and 3-OH GA metabolites displayed reduced accumulation in the striatum (**Figure 3F**). The levels of 3-OH GA in the serum of mice treated with the highest dose were also reduced **(Figure S3)**. Curiously, no correction of liver metabolites was observed with either dose (**Figure 3E**). We also analyzed whether the inhibition of AASS had any impact on the Lysine content. No differences in Lysine concentration neither in the liver nor in the striatum were detected when applied the highest dose, (**Figure S4**).

Overall, we detected a dose-dependent AASS lowering in the striatum after intravenous neonatal delivery of AAV9_miR_AASS with significant reduction of all the neurotoxic metabolites after the highest dose of AAV9_miR_AASS tested.

Neonatal delivery of AAV9_miR_AASS achieves long-term rescue of HLD-induced brain damage and improves lifespan of *Gcdh-/-* mice

Feeding *Gcdh-/-* mice at weaning with high lysine diet (HLD) or high protein diet induces a severe phenotype with high accumulation of the toxic metabolites GA and 3-OHGA, striatal neurodegeneration and limited mouse survival. [6,25,26] Since AAV9miR_AASS significantly reduced the accumulation of neurotoxic metabolites we also evaluated whether an intravenous neonatal delivery of AAV9_miR_AASS could ameliorate the harmful phenotype induced by HLD fed to *Gcdh-/-* mice. In wild-type mice, exposure to high protein diet has been reported to induce an increase in *AASS* mRNA content associated with higher enzyme activity. [27] Based on these observations we first analyzed the impact of a 4-days HLD on the AASS expression. Both WT and *Gcdh-/-* mice exposed to HLD displayed increased AASS protein levels in the liver as well as in the striatum (**Figure S5**). This agreed with the intracellular need to accelerate lysine degradation in a situation of lysine overload. However, this induction poses a very challenging scenario to assess the AAV9_miR_AASS treatment. Nevertheless, we proceeded to investigate the effects of AAV9_miR_AASS therapy at short- term (1-month) and long-term (6-months) post-administration upon HLD exposure (**Figure 4A**). For this, *Gcdh-/-* mice were injected with 5 x 10^{13} vg/kg of AAV9_miR_AASS at P1 and treated and non-treated animals were placed at weaning on HLD or standard diet (SD) for 4 days or 5-months. *Gcdh-/-* mice displayed typical symptoms associated to HLD exposure at this early stage of development and only 40% of them survive over the 6-month period, whereas 87% of *Gcdh-/-* mice treated with AAV9_miR_AASS survive during this time (**Figure 4B**). Body weight monitoring over the 6-months period revealed that HLD caused a 15% decrease in body weight during the first three days in untreated *Gcdh-/-* animals. Then, the average body weight increased but never reached the values of WT mice. Mice that received AAV9_miR_AASS showed a protection against the body weight decrease with a similar percentile of growth to that of WT mice until day 60 when they began to gain weight more

slowly, similar to the untreated group (**Figure 4C**). Some animals from all the groups were euthanized at 1- or 6-months post-treatment and analyzed for AASS expression and metabolite accumulation in the liver and striatum. Inhibition of AASS was very mild in the livers of AAV9_miR_AASS at 1-month, and no signs of metabolite correction were detected (**Figures 5A and 5B**). Despite undetectable AASS knockdown after 6-month post-treatment a noticeable reduction in the content of GA and a tendency towards less 3-OHGA accumulation was observed in the liver of treated mice (**Figures 5C and 5D**). Based on H&E staining, exposure to HLD, induced morphological alterations characterized by mild bile duct hyperplasia in portal triads after 4-days HLD and marked morphological changes in the parenchyma after 5-months of HLD, consisting of anisokaryosis mixed with multinucleated-appearing hepatocytes, intranuclear cytoplasmic invagination, apoptosis and infiltrates of inflammatory cells (**Figure 6A**). Under SD regime, animals euthanized at 1-month did not show any histological alterations, although at 6-months of age *Gcdh-/-* mice already displayed abnormal hepatocyte morphology with cytoplasmic vacuolation, and signs of hepatocyte intranuclear invagination and microgranulomas compatible with fatty liver. AAV9_miR_AASS treatment resulted in a very mild amelioration of liver morphology in mice exposed to SD diet for 6-months while it prevented the extensive liver damage induced by HLD (**Figure 6A**). In line with diffuse hepatocellular fatty change findings at *Gcdh-/-* mice on SD, the content of triglycerides in the serum of those mice were increased when compared to WT mice and were normalized by AAV9_miR_AASS therapy (**Figure 6B**). However, no clear alterations besides typical age-related effects were observed for Alkaline Phosphatase (ALP) and cholesterol in SD fed mice (**Figures 6C and 6D**). In animals fed with HLD, we observed an increase in ALP activity in *Gcdh-/-* mice independent of age with no sign of amelioration by the therapeutic vector. Consistent with marked liver alterations in *Gcdh-/-* with HLD exposure, cholesterol levels at 1- and 6-months and also triglycerides in 1-month group were significantly decreased in *Gcdh-/-* mice. Interestingly, treatment with AAV9_miR_AASS in *Gcdh-/-* mice on HLD

was associated with a partial rescue of cholesterol levels in serum, more clearly visible in 1-month animals.

Interestingly, in the striatum an AASS inhibition could be detected at the two time-points analyzed that correlated with a significant reduction in the GA and 3-OHGA content both at 1-and 6-months post-treatment (**Figures 7A-7D**). These results suggest that sustained inhibition of AASS for 6-months in the striatum could be sufficient to prevent HLD-induced metabolite accumulation.

Histopathological analysis of striatum confirmed previous observations of irregular vacuolation with increased vacuole size after chronic feeding with HLD for 5-months. [23,28] Interestingly, AAV9_miR_AASS prevented large vacuole formation (**Figure 8A**). Astrocyte damage analyzed by Glial Fibrillary Acidic Protein (GFAP) immunostaining showed abundant GFAP in *Gcdh*-/- mice fed with HLD, in line with a diet-induced gliosis, that was rescued by the therapy (**Figure 8B**). A progressive hypomyelination in *Gcdh*-/- mice fed with HLD was detected by Myelin Basic Protein (MBP) immunostaining after a 4 days- or 5-month diet regime. AAV9_miR_AASS therapy showed a tendency to prevent hypomyelination (**Figure 8C**).

Importantly, no virus- or sequence-related histopathological changes were observed neither in the striatum nor in the liver upon administration of the AAV9_miR_Sc suggesting no adverse events related to the vector (**Figure S6**).

Altogether, these results suggest that AAV9_miR_AASS effectively reduced AASS, by lowering the neurotoxic metabolite accumulation leading to therapeutic benefits in a diet-induced GA1 preclinical model.

Journal Pre-proof

DISCUSSION

GA1 is an inherited metabolic disorder due to mutations in the GCDH gene causing GCDH deficiency and an impairment in lysine degradation. This deficiency leads to disease-specific neurotoxic catabolites accumulation primarily in the central nervous system. [5,6] In the present work, we evaluated the potential of a substrate reduction therapy targeting AASS, the first enzyme of the lysine catabolic pathway, through the single administration of AAV9_miR_AASS in a preclinical mouse model of GA1. Our data demonstrate that systemic administration of the therapeutic vector at neonatal age prevented the accumulation of neurotoxic metabolites, mitigated tissue damage in *Gcdh-/-* mice subjected to a HLD regimen, and improved survival.

We initially designed four different artificial miRNAs embedded in the pri-miR16 scaffold for AASS silencing, as its genomic context has been described to be highly functional for inducing gene silencing. [29] Previous studies have shown that pri-miR-16 was an optimal RNA substrate both in functional assays [30,31] and at structural level in complex with miRNA processing factors, [32,33] suggesting pri-miR-16 adequacy as a robust backbone. The use of artificial miRNAs as an RNA interference approach was selected beyond siRNA or pol-III driven shRNAs for its feasibility of inducing a highly efficient and stable targeted silencing avoiding any toxicity associated to high levels of mature inhibitory RNAs. [34,35] We demonstrated in both human and murine cell lines the capacity of the candidate miR_4 of reducing AASS mRNA, protein expression and enzymatic activity, slowing down the catabolism of lysine. Also, miR_4 targeting specificity was assessed by miR_4_Sc assays, confirming that miR_4 guide strand was the responsible for AASS silencing.

In the *in vivo* studies performed, AAV serotype 9 capsid was selected due to its tropism to the brain, which is the mainly target tissue in GA1. [36] We also worked with a modified serotype 9 AAV (AAV9P31), which has been reported to be very efficient in crossing the

blood brain barrier in adult mice compared to AAV9. [20,37] AAV9_miR_AASS intravenous administration at neonatal (P1) age but not at young-adult (P30) showed optimal biodistribution and silencing efficiency of AASS in striatum. This could be related to the fact that systemic AAV9 administration at advanced post-natal stages has limited transduction to CNS, due to the reduced capacity of AAV9 to optimally cross the BBB. [23,38] In contrast, at neonatal stages, when BBB is not yet fully formed, transduction of the vector into the CNS can be achieved. [39,40] Alternatively, AAV9 variants with enhanced CNS transduction could be used. In fact, we observed that the systemic administration of the AAV9P31_miR_AASS in P30 mice efficiently reached both liver and striatum and induced AASS downregulation. Although this modified serotype raises the problem of the lack of BBB bypass in humans, limiting its translational potential, at the same time highlights the need to expand efforts to identify BBB-penetrant capsid variants for clinical use. [20,41]

To increase CNS-targeted delivery in young adult mice, locoregional administration via cisterna magna could be an option. [42] AAV9_miR_AASS delivery showed improved transduction and AASS targeting to striatum compared to IV administration, however it was insufficient to reduce metabolite accumulation, at least 1-month post-treatment, again highlighting either the use of AAV9P31_miR_AASS serotype or the neonatal delivery of AAV9_miR_AASS as the optimal strategies to correct alterations in the striatum of GA1 mice.

Systemic administration of AAV9_miR_AASS in neonatal mice was in fact more efficient in the striatum than the liver, since at 1-month post-treatment we already observed the preventive effect on the accumulation of metabolites GA and 3-OHGA in the striatum at all the conditions studied, whereas in the liver we only observed the preventive effect after 6-months post-treatment, again supporting the relevance of an early administration time for impacting the CNS with AAV9 vectors (**Figure S7**). At the same time, we have to consider the effect of organ growth in diluting the inhibition of AASS in the liver,

345 although interestingly the low metabolites concentrations observed at long-term in
346 AAV9_miR_AASS treated mice indicated that even small inhibition of AASS can have
347 an impact on the accumulation of metabolites for an extended period of time. Recent
348 data, on a series of transplantation experiments have shown that hepatic lysine
349 catabolism directly affects the accumulation of toxic metabolites in the brain of a GA1
350 mouse model. [11] Our strategy of neonatal delivery was particularly focused in targeting
351 the brain and although we also had some effects in the liver we are not able to
352 discriminate about the individual contribution from either organ.

353 Exposure of *Gcdh-/-* mice to HLD, led to biochemical and neuropathological alterations
354 that resemble the encephalopathic episodes that occur in individuals with GA1 as
355 previously described. [25,26] Of notice, HLD overload, resulted in elevated levels of AASS
356 protein expression in liver and striatum in both, WT and *Gcdh-/-* mice consistent with
357 previous descriptions, reporting post-translational regulation of AASS under high lysine
358 or high protein conditions in several animals and plant species. [27,43] Despite this side
359 effect, neonatal administration of AAV9_miR_AASS in *Gcdh-/-* mice exposed to HLD led
360 to significant AASS and metabolite reduction in striatum, up to 6-months post-treatment,
361 suggesting the potential of the therapy to counteract the induction of AASS by HLD.

362 Striatum histopathological analysis revealed progressive vacuole formation bordered by
363 reactive astrocytes and loss of myelin in *Gcdh-/-* mice exposed to HLD for five months,
364 compared to SD groups in line with previous reports.[25,44–46] Interestingly,
365 AAV9_miR_AASS treated mice almost completely rescued the neurological phenotype,
366 suggesting that therapy provides a neuroprotective effect against HLD-induced striatal
367 injury.

368 The HLD feeding also impacted liver pathology and functionality in the GA1 model.
369 Remarkable hepatotoxic effects were observed in *Gcdh-/-* mice, with signs of hepatocyte
370 damage and generalized inflammation after long-term exposure. Probably, early events,

observed after 4 days of HLD already indicating liver dysfunction such as alterations in ALP and cholesterol levels contributed to the histopathological defects observed after 5 months of continuous HLD. Altered cholesterol levels are frequently found in the context of hepatic diseases, since the liver is a central regulator of cholesterol homeostasis.[47] Interestingly, our results showed an amelioration of cholesterol decrease in the AAV9_miR_AASS treated group, suggesting that impairment of metabolism was less pronounced, which was also supported by the histopathological findings in the liver of *Gcdh-/-* treated mice 6-months post-treatment. Moreover, aging of GA1 mice under SD already altered liver function, showing elevated triglycerides levels and hepatocellular fatty changes observed in 6-months old mice suggesting that long-term *Gcdh* deficiency effects on liver metabolism, cause impaired cellular energy metabolism [23,48]. Interestingly, AAV9_miR_AASS prevented triglycerides accumulation, in line with the halt in toxic metabolite accumulation.

The current data indicate that AASS inhibition by artificial miRNA could be postulated as a therapy for GA1. AAV9_miR_AASS neonatal systemic administration has proven to be efficient in the transduction to the target tissues of GA1, preventing metabolites accumulation, protecting against neuropathology and extending survival. Considering that GA1 is characterized by an early onset of the disease, the present therapeutic proposal would allow an early non-invasive intervention before the patient is at risk of suffering acute encephalopathic crises. Being an optimal scenario the administration of this treatment after disease detection through the neonatal screening programs. Furthermore, this strategy of substrate reduction could be also considered as a therapeutic approach for pyridoxine-dependent epilepsy (PDE; MIM # 266100) [10,12], a disease of lysine metabolism due to defects on the third enzyme of the catabolic pathway (AASA), in which the accumulation of toxic metabolites are responsible for the appearance of neurological symptoms. Thus, by avoiding the catabolism of lysine through the inhibition of the initial step of this metabolic pathway, the accumulation of

neurotoxic metabolites would be reduced, and consequently be considered an attractive proposal for GA1 and PDE therapies.

Journal Pre-proof

401 MATERIALS AND METHODS

402

403 **AASS target sequences and DNA constructs.** *Homo sapiens* and *Mus musculus*
404 *AASS* and Aass transcripts (ENST00000417368.7 and ENSMUST00000031707.14)
405 obtained from http://www.ensembl.org were used to identify target sequences for AASS
406 knockdown (miR_AASS). To generate the pri-miR_AASS constructs, miRNA sequences
407 targeting *AASS*/Aass transcripts were embedded into the human pri-miR-16 backbone;
408 300bp of double-stranded DNA fragments were obtained as gBlocks™ Gene Fragments
409 (Integrated DNA Technologies) and cloned into the pAAV-CA (Plasmid # 69616,
410 Addgene), containing the CAG promoter (chimeric promoter with the CMV enhancer and
411 the chicken β-actin promoter) to generate 4 plasmids pAAV9-miR_AASS with
412 sequences 1-4. A control pAAV9-miR_Sc plasmid was generated with a scrambled
413 organization of sequence 4.
414 Luciferase reporter constructs with human and mouse *AASS/Aass* cDNA sequences
415 were obtained by cloning the cDNA fragments in the 3'UTR of the *Renilla Luciferasa*
416 gene of the psiCHECK-2 vector (Promega).
417 All plasmid sequences were validated by Sanger sequencing.

418

419 **AAV vector generation.** AAV9_miR_AASS, and AAV9_miR_Sc viral vectors were
420 generated from pAAV9-miR_AASS and pAAV9-miR_Sc backbones in an AAV9 capsid.
421 AAV vectors were produced according to standard procedures at the Viral Vector
422 Production Unit (UPV), Autonomous University of Barcelona.
423 AAV9P31_miR_AASS vectors were generated from pAAV9_miR_AASS backbones in
424 the AAV9P31 modified capsid and produced at CIMA Universidad de Navarra.

425

426 **Cell culture and transfections.** HEK293T, NIH 3T3 and SH-SY5Y cell lines were
427 obtained from the American Type Culture Collection (ATCC). miR_AASS and miR_Sc
428 cell lines were established by co-transfecting the parental cells with pAAV9-miR_AASS

or pAAV9-miR_Sc expression constructs and the plasmid p_BABE_puro (Addgene) at ratio 10:1. At 48 hours after the co-transfection, cells were selected with puromycin (2.5 µg/ml), and individual clones were subsequently isolated and expanded. Three clones for each cell line were used for the validation experiments.

All cell lines grew as adherent cultures and were maintained in a humidified atmosphere of 5% CO2 at 37ºC. HEK293T and NIH 3T3 cells were cultured in DMEM (Gibco ™ Dulbecco's Modified Eagle Medium; Thermo Fisher Scientific), and SH-SY5Y in Advanced DMEM/F-12 (Life Technologies) supplemented with 10% serum fetal bovine serum (Gibco Fetal Bovine Serum; Thermo Fisher Scientific), 2 mM glutamine, 100 U/mL penicillin and 100 mg/mL streptomycin. Cells obtained from the ATCC were expanded and frozen. Every 2 months cells were plated from the original batch. Cells were not authenticated by the authors. Interspecies contamination was tested by PCR routinely.

Transfections were performed with Lipofectamine 3000 reagent (Invitrogen) for HEK 293T and NIH 3T3, and CalPhos™ Mammalian Transfection Kit (Clontech® Laboratories) for SH-SY5Y, according to the manufacturer's instructions.

Luciferase assays. HEK293T cells were co-transfected with pAAV-miR_AASS expression constructs and luciferase reporters that contains both the RLuc gene fused to mouse and human *AASS/Aass* cDNA and the FLuc gene. Transfected cells were assayed at 72h post-transfection and cell lysates were analysed using Dual-Luciferase Reporter Assay System (Promega), according to the manufacturer's instructions.

Indirect measurement of AASS activity. NIH 3T3 and SH-SY5Y cells were cultured in the absence or presence of 10 mM lysine for 72h, to stimulate the catabolism of the amino acid, and therefore the activity of AASS. Cell lysates were obtained after adding a lysis buffer (Passive Lysis Buffer, Promega) on the cell culture and incubating them at -80ºC for 1h. NADPH consumption was analyzed using a bioluminescence assay,

NAD(P)H-Glo™ Detection System (Promega) according to the manufacturer's instructions.

Mature miR_AASS quantification. microRNA isolation was performed from frozen tissue using miRNeasy® Mini Kit (Qiagen). To determine miR_AASS mature microRNA molecule levels, the TaqMan MicroRNA Reverse Transcription kit (Applied Biosystems) and gene specific RT primers to target miR_AASS mature guide strand were used. As a housekeeping, miR_U6 was also amplified using specific RT primers. Mature miR_AASS and miR_U6 molecules were quantified by performing RT-qPCRs using TaqMan Universal PCR MasterMix (Thermo Fischer Scientific), on a QuantStudio 7 (Applied Biosystems) thermocycler.

RT-qPCR of *AASS/Aass* mRNA.

Total RNA extraction was performed using RNeasy® Min Kit (Qiagen). The synthesis of single-stranded complementary DNA (cDNA) was performed using PrimeScript RT-PCR Kit (Takara) according to the manufacturer's protocols.The levels of mRNA expression were analysed by quantitative PCR using specific primers to determine AASS and HPRT as a housekeeping (Table S1). PCR was performed using LightCycler® 480 SYBR Green (Roche) on a QuantStudio 7 (Applied Biosystems) thermocycler.

Western blot analysis. Protein extracts were obtained using lysis buffer (10 mM Tris-HCl [pH 6.8], 4% SDS, and 20% glycerol) containing 1% Complete Mini Protease Inhibitor (Roche). Lysates were boiled for 10 min at 98ºC and centrifuged 5 min at 16,000 x *g*. Protein concentration was determined by BCA Protein Assay kit (ThermoFisher Scientific). Protein samples were resolved in 10% SDS-PAGE and transferred to PVDF membranes by standard methods. Membranes were blocked with TBS-Tween 10% milk (1 h at room temperature), immunoblotted with the corresponding antibody (Anti-AASS HPA020734; Anti-GAPDH ABS16) diluted in TBS-Tween 1% milk,

rinsed with TBS-Tween, and incubated with a polyclonal goat anti-rabbit HPR-conjugated antibody (1/2000 in TBS-Tween 1% milk, 1h at room temperature). Antibody labelling was detected by ECL Amersham Prime Western Blotting Detection Reagent (GE Healthcare Life Sciences).

Biochemical analysis. Tissue extracts were obtained through mechanical homogenization. Briefly, liver and striatum from mice were Dounce homogenized (20 strokes) in lysis buffer (225mM Manitol, 75mM Sucrose, 10mM Tris-HCl and 0.1mM EDTA) on ice. Tissue homogenates were centrifuged twice at 650g for 20 min at 4°C to remove cell debris and nuclei. Protein concentration was determined using a BCA assay. For glutaric acid and 3-OH-glutaric analysis, an aqueous solution containing the deuterium labeled internal standards GA-d4 and 3-OH-GA-d5, was added to the homogenized tissue or serum samples. Compounds were extracted using an Oasis HLB 96-well Plate and eluted using an acetonitrile/methanol (90/10) phase, after formic acid at 0,4% solution was added to facilitate the ionization. Chromatographic separation was done on an ACQUITY UPLC system (H-Class, Waters, MA, USA)-XevoTQS with an ACQUITY Premier BEH C18 Column (1.7 µm, 2.1 x 100 mm). The flow rate was set to 320 µL min^{-1} using a binary mixture of solvent A (water with 0.1% formic acid) and solvent B (methanol with 0.1% formic acid). Values were quantified with Targetlynx Software (Walters) using a calibration curve and normalized for protein content in case of tissues. Lysine was measured using amino acid profile analysis by ultra-high-performance liquid chromatography-tandem mass spectrometry (UHPLC-MS/MS) with the MassChrom® AA analysis kit. Briefly, liver and striatum tissue were homogenized in 100 µL of ultrapure water. Then, 25 µL of the homogenate were mixed with 50 µL of a labeled amino acid mixture (including labeled lysine), used as an internal standard, and 375 µL of a protein precipitation reagent. After centrifugation, 6 µL of the supernatant were injected into the UHPLC-MS/MS system (Shimadzu Nexera UHPLC – Sciex 5500+ QTRAP, AB SCIEX, USA). Chromatographic separation was performed using an analytical column

(Chromsystems, CH-75100, Gräfelfing, Germany). The mobile phase gradient, flow rate, and mass spectrometry parameters were used as specified in the kit protocol. The mass spectrometer operated with electrospray ionization in positive ion mode using multiple reaction monitoring (MRM). Calibration curves were constructed by linear regression analysis of the ratio of the peak area of each amino acid to that of the corresponding labeled internal standard. Quantification was performed using SciexOS software (Framingham, USA), and results were expressed in nmol/mg of protein, after protein normalization.

Animal procedures. *Gcdh-/-* mice were purchased from the Mutant Mouse Resource and Research Center (MMRRC) strain ID 34368 and maintained in an SPF animal facility in a 12h dark-light cycle. Mice were fed ad libitum with a standard diet (SD) or a high lysine diet (HLD) 4,7% Lys (ENVIGO) when stated. Animals were placed in HLD at 3-week-old weanling. Blood samples were collected by intracardiac puncture and mice were sacrificed 1- or 6-months post-treatment.

Gcdh-/- mice were injected in the temporal vein (neonatal), tail vein (young adult) or cisterna magna with $5x10^{13}$ vg/kg or $7,5x10^{12}$ vg/kg of AAV9_miR_AASS, AAV9_miR_Sc or AAV9P31_miR_AASS**.** Neonatal injections and cisterna magna administrations were performed following the previously described protocol [22,49].

Animal procedures met the guidelines of European Community Directive 86/609/EEC and the local legislation (Decret 214/1997 of July 20th by the Department d'Agricultura, Ramaderia i Pesca de la Generalitat de Catalunya) under the approval of the Experimental Animal and Ethical Committee of the University of Barcelona (CEEA).

Histological preparation and Immunohistochemistry analysis. Mice were transcardiacally perfused with 1% PBS followed by 4% paraformaldehyde. Brains and

livers were removed and postfixed in 4% paraformaldehyde for 24h at 4ºC and embedded in paraffin. Serial 6 µm brain coronal and liver sections were collected on glass slides and standard hematoxylin and eosin stainings were performed.

For IHC sections were processed for antigen retrieval in citrate buffer (Citrate Buffer 10x pH 6.0 10x Sigma-Aldrich) at 100ºC (boiling point) for 5 min in a pressure cooker. Sections were treated with a blocking solution (PBS 1x, 10% FBS, 1% BSA, 0.3% triton X-100) for 1'5 h at room temperature and incubated overnight at 4ºC with primary antibodies (Anti-Glial Fibrillary Acidic Protein (GFAP), G3893, Sigma-Aldrich; Anti-NeuN, clone A60, Sigma-Aldrich and anti-Myelin Basic Protein (MBP), clone SMI 94, Biolegend) diluted in PBS with 0.1% BSA. Endogenous peroxidase was blocked with Dual Endogenous Enzyme Block (Dako) for 10 min at room temperature. The reaction was developed using Dako EnVision + Dual Link System-HRP (DAB+) (Dako), and tissues were counterstained with Harris hematoxylin (Panreac). Stained sections were visualized with an Olympus BX51 vertical microscope and digitalized with a ScanScope.

Serum clinical biochemistry analysis: Frozen serum samples were thawed, diluted 1:2 with deionized water throroughly mixed and afterwards centrifuged (5000xg, 10 Min at 8°C) to remove clots before being analyzed for alkaline phosphatase activities, cholesterol and triglyceride levels using an AU480 Clinical chemistry analyzer (Beckman Coulter) and test kits provided by Beckman Coulter as previously described [50]

Statistical analysis. Experimental data are represented by the mean ± SEM of at least three independent experiments. Statistical analysis was performed on GraphPad Prism v8.0.1 (GraphPad Software). Statistical differences were evaluated using a 2-tailed non-parametric Mann-Whitney test. $P < 0.05$ was taken as the level of significance. Mice survival was analyzed by the Kaplan-Meier method and evaluated with a long-rank (Mantel-Cox) test.

Journal Pre-proof

DATA AVAILABILITY

Data are available within the published article and supplemental files. Additional data are available from corresponding author on reasonable request.

ACKNOWLEDGEMENTS

We are indebted to the Biobank and Image core facilities of IDIBAPS for technical help and to the Unitat d'Experimentació Animal del Campus Clínic – CCiTUB for animal studies. We acknowledge all members of the CHARLIE Consortium *(www.charlie.science)* for their helpful discussions. This project received support from Instituto de Salud Carlos III (ISCIII) under the frame of E-Rare-3, the ERA-Net for Research on Rare Diseases, EJPRD grant nr: 825575. This work was also supported by grants from the CIVP19A5949-Fundación Ramon Areces, ACCI-CIBERER and PID2020-119692RB-C22 Spanish Ministerio de Ciencia e Innovación, with partial support from the Generalitat de Catalunya SGR21/01169 and from ISCIII RICORS TERAV RD21/0017/0012 and RD21/0017/0034. CIBERER is an initiative of the ISCIII. The research leading to these results has also received funding from "la Caixa" Foundation under agreement LCF/PR/SP23/52950009. We also acknowledge the support of CERCA Programme/Generalitat de Catalunya. AM-B was recipient of a PIF-Salut predoctoral contract from Generalitat de Catalunya, Spain. This work was developed at the Centro Esther Koplowitz and Section of Inborn Errors of Metabolism-Hospital Clinic, Barcelona, Spain. Schemes and the graphical abstract were created with Biorender.com.

AUTHOR CONTRIBUTIONS

ES-B, designed and performed most of the experiments, contributed to manuscript writing and prepared the figures, AM-B contributed with the mouse studies, JG-V guide

the metabolite analysis, MP contributed with experiments, XB-DR, PM and GG-A contributed with the AAV design and generation. PdSB, BR, MHA and VG-D analyzed the clinical biochemistry parameters and liver histology, AR and FT provided GA1 pathology expertise and contributed to manuscript writing, CvK coordinated the CHARLIE consortium and contributed with data discussion, CF coordinated the study and wrote the manuscript.

DECLARATION OF INTERESTS

The authors declare no competing interests.

KEYWORDS

Glutaric Aciduria, gene therapy, artificial miRNAs, AAVs

REFERENCES

1. Goodman, S.I., Markey, S.P., Moe, P.G., Miles, B.S., and Teng, C.C. (1975). Glutaric aciduria; a “new” disorder of amino acid metabolism. Biochem Med *12*, 12–21. https://doi.org/10.1016/0006-2944(75)90091-5.
2. Kölker, S., Garbade, S.F., Boy, N., Maier, E.M., Meissner, T., Mühlhausen, C., Hennermann, J.B., Lücke, T., Häberle, J., Baumkötter, J., et al. (2007). Decline of acute encephalopathic crises in children with glutaryl-CoA dehydrogenase deficiency identified by newborn screening in Germany. Pediatr Res *62*, 357–363. https://doi.org/10.1203/PDR.0B013E318137A124.
3. Boy, N., Mengler, K., Thimm, E., Schiergens, K.A., Marquardt, T., Weinhold, N., Marquardt, I., Das, A.M., Freisinger, P., Grünert, S.C., et al. (2018). Newborn

screening: A disease-changing intervention for glutaric aciduria type 1. Ann Neurol *83*, 970–979. https://doi.org/10.1002/ANA.25233.

4. Hedlund, G.L., Longo, N., and Pasquali, M. (2006). Glutaric acidemia type 1. Am J Med Genet C Semin Med Genet *142C*, 86–94. https://doi.org/10.1002/AJMG.C.30088.

5. Jafari, P., Braissant, O., Bonafé, L., and Ballhausen, D. (2011). The unsolved puzzle of neuropathogenesis in glutaric aciduria type I. Mol Genet Metab *104*, 425–437. https://doi.org/10.1016/J.YMGME.2011.08.027.

6. Kölker, S., Sauer, S.W., Surtees, R.A.H., and Leonard, J. V. (2006). The aetiology of neurological complications of organic acidaemias--a role for the blood-brain barrier. J Inherit Metab Dis *29*, 701–704. https://doi.org/10.1007/S10545-006-0415-8.

7. Harting, I., Neumaier-Probst, E., Seitz, A., Maier, E.M., Assmann, B., Baric, I., Troncoso, M., Mühlhausen, C., Zschocke, J., Boy, N.P.S., et al. (2009). Dynamic changes of striatal and extrastriatal abnormalities in glutaric aciduria type I. Brain *132*, 1764–1782. https://doi.org/10.1093/brain/awp112.

8. Boy, N., Mühlhausen, C., Maier, E.M., Ballhausen, D., Baumgartner, M.R., Beblo, S., Burgard, P., Chapman, K.A., Dobbelaere, D., Heringer-Seifert, J., et al. (2023). Recommendations for diagnosing and managing individuals with glutaric aciduria type 1: Third revision. J Inherit Metab Dis *46*, 482–519. https://doi.org/10.1002/JIMD.12566.

9. Boy, N., Mengler, K., Heringer-Seifert, J., Hoffmann, G.F., Garbade, S.F., and Kölker, S. (2021). Impact of newborn screening and quality of therapy on the neurological outcome in glutaric aciduria type 1: a meta-analysis. Genet Med *23*, 13–21. https://doi.org/10.1038/S41436-020-00971-4.

10. Leandro, J., Dodatko, T., DeVita, R.J., Chen, H., Stauffer, B., Yu, C., and Houten, S.M. (2020). Deletion of 2-aminoadipic semialdehyde synthase limits metabolite

accumulation in cell and mouse models for glutaric aciduria type 1. J Inherit Metab Dis *43*, 1154–1164. https://doi.org/10.1002/JIMD.12276.

11. Barzi, M., Johnson, C.G., Chen, T., Rodriguiz, R.M., Hemmingsen, M., Gonzalez, T.J., Rosales, A., Beasley, J., Peck, C.K., Ma, Y., et al. (2023). Rescue of glutaric aciduria type I in mice by liver-directed therapies. Sci Transl Med *15*. https://doi.org/10.1126/scitranslmed.adf4086.

12. Leandro, J., and Houten, S.M. (2020). The lysine degradation pathway: Subcellular compartmentalization and enzyme deficiencies. Preprint at Academic Press Inc., https://doi.org/10.1016/j.ymgme.2020.07.010.

13. Cabrera, G.T., and Mueller, C. (2016). Design of shRNA and miRNA for Delivery to the CNS. Methods in Molecular Biology *1382*, 67–80. https://doi.org/10.1007/978-1-4939-3271-9_5.

14. Bofill-De Ros, X., and Gu, S. (2016). Guidelines for the optimal design of miRNA-based shRNAs. Methods *103*, 157. https://doi.org/10.1016/J.YMETH.2016.04.003.

15. Becker, W.R., Ober-Reynolds, B., Jouravleva, K., Jolly, S.M., Zamore, P.D., and Greenleaf, W.J. (2019). High-Throughput Analysis Reveals Rules for Target RNA Binding and Cleavage by AGO2. Mol Cell *75*, 741. https://doi.org/10.1016/J.MOLCEL.2019.06.012.

16. Koeller, D.M., Woontner, M., Crnic, L.S., Kleinschmidt-Demasters, B., Stephens, J., Hunt, E.L., and Goodman, S.I. (2002). Biochemical, pathologic and behavioral analysis of a mouse model of glutaric acidemia type I. Hum Mol Genet *11*, 347–357. https://doi.org/10.1093/HMG/11.4.347.

17. Mohamed, A.A., Wang, P.Y., Bartel, D.P., and Vos, S.M. (2024). The structural basis for RNA slicing by human Argonaute2. Cell Rep *44*, 115166. https://doi.org/10.1016/J.CELREP.2024.115166.

18. Shay, T.F., Sullivan, E.E., Ding, X., Chen, X., Kumar, S.R., Goertsen, D., Brown, D., Crosby, A., Vielmetter, J., Borsos, M., et al. (2023). Primate-conserved

carbonic anhydrase IV and murine-restricted LY6C1 enable blood-brain barrier crossing by engineered viral vectors. Sci Adv *9*. https://doi.org/10.1126/SCIADV.ADG6618/SUPPL_FILE/SCIADV.ADG6618_SM.PDF.

19. Tafer, H., Ameres, S.L., Obernosterer, G., Gebeshuber, C.A., Schroeder, R., Martinez, J., and Hofacker, I.L. (2008). The impact of target site accessibility on the design of effective siRNAs. Nat Biotechnol *26*, 578–583. https://doi.org/10.1038/NBT1404,.

20. Bunuales, M., Garduno, A., Chillon, M., Bosch, A., Gonzalez-Aparicio, M., Espelosin, M., Garcia-Gomara, M., Rico, A.J., Garcia-Osta, A., Cuadrado-Tejedor, M., et al. (2024). Characterization of brain transduction capability of a BBB-penetrant AAV vector in mice, rats and macaques reveals differences in expression profiles. Gene Ther *31*, 455–466. https://doi.org/10.1038/s41434-024-00466-w.

21. Sarshad, A.A., Juan, A.H., Muler, A.I.C., Anastasakis, D.G., Wang, X., Genzor, P., Feng, X., Tsai, P.F., Sun, H.W., Haase, A.D., et al. (2018). Argonaute-miRNA Complexes Silence Target mRNAs in the Nucleus of Mammalian Stem Cells. Mol Cell *71*, 1040. https://doi.org/10.1016/J.MOLCEL.2018.07.020.

22. Lampe, S.E.G., Kaspar, B.K., and Foust, K.D. (2014). Intravenous injections in neonatal mice. J Vis Exp. https://doi.org/10.3791/52037.

23. Mateu-Bosch, A., Segur-Bailach, E., Muñoz-Moreno, E., Barallobre, M.J., Arbonés, M.L., Gea-Sorlí, S., Tort, F., Ribes, A., García-Villoria, J., and Fillat, C. (2024). Systemic delivery of AAV-GCDH ameliorates HLD-induced phenotype in a glutaric aciduria type I mouse model. Mol Ther Methods Clin Dev *32*, 101276. https://doi.org/10.1016/J.OMTM.2024.101276.

24. Arabi, F., Mansouri, V., and Ahmadbeigi, N. (2022). Gene therapy clinical trials, where do we go? An overview. Biomedicine & Pharmacotherapy *153*, 113324. https://doi.org/10.1016/J.BIOPHA.2022.113324.

25. Zinnanti, W.J., Lazovic, J., Wolpert, E.B., Antonetti, D.A., Smith, M.B., Connor, J.R., Woontner, M., Goodman, S.I., and Cheng, K.C. (2006). A diet-induced mouse model for glutaric aciduria type I. Brain *129*, 899–910. https://doi.org/10.1093/BRAIN/AWL009.

26. Zinnanti, W.J., Lazovic, J., Housman, C., Lanoue, K., O'Callaghan, J.P., Simpson, I., Woontner, M., Goodman, S.I., Connor, J.R., Jacobs, R.E., et al. (2007). Mechanism of age-dependent susceptibility and novel treatment strategy in glutaric acidemia type I. J Clin Invest *117*, 3258–3270. https://doi.org/10.1172/JCI31617.

27. Kiess, A.S., Cleveland, B.M., Wilson, M.E., Klandorf, H., and Blemings, K.P. (2008). Protein-induced alterations in murine hepatic alpha-aminoadipate delta-semialdehyde synthase activity are mediated posttranslationally. Nutrition Research *28*, 859–865. https://doi.org/10.1016/J.NUTRES.2008.09.010.

28. Amaral, A.U., Seminotti, B., da Silva, J.C., de Oliveira, F.H., Ribeiro, R.T., Leipnitz, G., Souza, D.O., and Wajner, M. (2019). Acute lysine overload provokes marked striatum injury involving oxidative stress signaling pathways in glutaryl-CoA dehydrogenase deficient mice. Neurochem Int *129*. https://doi.org/10.1016/J.NEUINT.2019.104467.

29. Watanabe, C., Cuellar, T.L., and Haley, B. (2016). Quantitative evaluation of first, second, and third generation hairpin systems reveals the limit of mammalian vector-based RNAi. RNA Biol *13*, 25–33. https://doi.org/10.1080/15476286.2015.1128062.

30. Fang, W., and Bartel, D.P. (2015). The menu of features that define primary microRNAs and enable de novo design of microRNA genes. Mol Cell *60*, 131. https://doi.org/10.1016/J.MOLCEL.2015.08.015.

31. Bofill-De Ros, X., Hong, Z., Birkenfeld, B., Alamo-Ortiz, S., Yang, A., Dai, L., and Gu, S. (2022). Flexible pri-miRNA structures enable tunable production of 5'

isomiRs. RNA Biol *19*, 279–289. https://doi.org/10.1080/15476286.2022.2025680.

32. Jin, W., Wang, J., Liu, C.P., Wang, H.W., and Xu, R.M. (2020). Structural Basis for pri-miRNA Recognition by Drosha. Mol Cell *78*, 423-433.e5. https://doi.org/10.1016/J.MOLCEL.2020.02.024.

33. Partin, A.C., Zhang, K., Jeong, B.C., Herrell, E., Li, S., Chiu, W., and Nam, Y. (2020). Cryo-EM Structures of Human Drosha and DGCR8 in Complex with Primary MicroRNA. Mol Cell *78*, 411-422.e4. https://doi.org/10.1016/J.MOLCEL.2020.02.016.

34. Lam, J., Chow, M., Zhang, Y., and Leung, S. (2015). siRNA Versus miRNA as Therapeutics for Gene Silencing. Molecular Therapy *4*, e252. https://doi.org/10.1038/mtna.2015.23.

35. McBride, J.L., Boudreau, R.L., Harper, S.Q., Staber, P.D., Monteys, A.M., Martins, I., Gilmore, B.L., Burstein, H., Peluso, R.W., Polisky, B., et al. (2008). Artificial miRNAs mitigate shRNA-mediated toxicity in the brain: implications for the therapeutic development of RNAi. Proc Natl Acad Sci U S A *105*, 5868–5873. https://doi.org/10.1073/PNAS.0801775105.

36. Dufour, B.D., and McBride, J.L. (2016). Intravascular AAV9 Administration for Delivering RNA Silencing Constructs to the CNS and Periphery. Methods in Molecular Biology *1364*, 261–275. https://doi.org/10.1007/978-1-4939-3112-5_21.

37. Zhang, R., Liu, Y., Yu, F., Xu, G., Li, L., Li, B., and Lou, Z. (2024). Structural basis of the recognition of adeno-associated virus by the neurological system-related receptor carbonic anhydrase IV. PLoS Pathog *20*, e1011953. https://doi.org/10.1371/JOURNAL.PPAT.1011953.

38. Foust, K.D., Nurre, E., Montgomery, C.L., Hernandez, A., Chan, C.M., and Kaspar, B.K. (2009). Intravascular AAV9 preferentially targets neonatal neurons

Journal Pre-proof

and adult astrocytes. Nat Biotechnol *27*, 59–65. https://doi.org/10.1038/NBT.1515.

39. Słyk, Ż., Stachowiak, N., and Małecki, M. (2024). Recombinant Adeno-Associated Virus Vectors for Gene Therapy of the Central Nervous System: Delivery Routes and Clinical Aspects. Biomedicines *12*, 1523. https://doi.org/10.3390/BIOMEDICINES12071523.

40. Lowenstein, P.R. (2009). Crossing the Rubicon. Nat Biotechnol *27*, 42. https://doi.org/10.1038/NBT0109-42.

41. Schuster, D.J., Dykstra, J.A., Riedl, M.S., Kitto, K.F., Belur, L.R., Scott McIvor, R., Elde, R.P., Fairbanks, C.A., and Vulchanova, L. (2014). Biodistribution of adeno-associated virus serotype 9 (AAV9) vector after intrathecal and intravenous delivery in mouse. Front Neuroanat *8*. https://doi.org/10.3389/FNANA.2014.00042.

42. Haery, L., Deverman, B.E., Matho, K.S., Cetin, A., Woodard, K., Cepko, C., Guerin, K.I., Rego, M.A., Ersing, I., Bachle, S.M., et al. (2019). Adeno-Associated Virus Technologies and Methods for Targeted Neuronal Manipulation. Front Neuroanat *13*, 493120. https://doi.org/10.3389/FNANA.2019.00093/BIBTEX.

43. Foster, A.R., Scislowski, P.W.D., Ian Harris, C., and Fuller, M.F. (1993). Metabolic response of liver lysine α-ketoglutarate reductase activity in rats fed lysine limiting or lysine excessive diets. Nutrition Research *13*, 1433–1443. https://doi.org/10.1016/S0271-5317(05)80792-4.

44. Wajner, M., Amaral, A.U., Leipnitz, G., and Seminotti, B. (2019). Pathogenesis of brain damage in glutaric acidemia type I: Lessons from the genetic mice model. Int J Dev Neurosci *78*, 215–221. https://doi.org/10.1016/J.IJDEVNEU.2019.05.005.

45. Cudré-Cung, H.P., Remacle, N., do Vale-Pereira, S., Gonzalez, M., Henry, H., Ivanisevic, J., Schmiesing, J., Mühlhausen, C., Braissant, O., and Ballhausen, D. (2019). Ammonium accumulation and chemokine decrease in culture media of

Gcdh-/- 3D reaggregated brain cell cultures. Mol Genet Metab *126*, 416–428. https://doi.org/10.1016/J.YMGME.2019.01.009.

46. Olivera-Bravo, S., Seminotti, B., Isasi, E., Ribeiro, C.A., Leipnitz, G., Woontner, M., Goodman, S.I., Souza, D., Barbeito, L., and Wajner, M. (2019). Long Lasting High Lysine Diet Aggravates White Matter Injury in Glutaryl-CoA Dehydrogenase Deficient (Gcdh-/-) Mice. Molecular Neurobilogy *56*, 648–657. https://doi.org/10.1007/S12035-018-1077-X.

47. Luo, J., Yang, H., and Song, B.L. (2020). Mechanisms and regulation of cholesterol homeostasis. Nat Rev Mol Cell Biol *21*, 225–245. https://doi.org/10.1038/S41580-019-0190-7.

48. Ferreira, G.D.C., Viegas, C.M., Schuck, P.F., Tonin, A., Ribeiro, C.A.J., Coelho, D.D.M., Dalla-Costa, T., Latini, A., Wyse, Â.T.S., Wannmacher, C.M.D., et al. (2005). Glutaric acid administration impairs energy metabolism in midbrain and skeletal muscle of young rats. Neurochem Res *30*, 1123–1131. https://doi.org/10.1007/S11064-005-7711-9.

49. Joshi, K., Kirby, A., Niu, J., and Vanderhorst, V. (2022). Stereotaxic Surgical Approach to Microinject the Caudal Brainstem and Upper Cervical Spinal Cord via the Cisterna Magna in Mice. Journal of Visualized Experiments *2022*. https://doi.org/10.3791/63344.

50. Rathkolb, B., Fuchs, H., Gailus-Durner, V., Aigner, B., Wolf, E., and Hrabě de Angelis, M. (2013). Blood Collection from Mice and Hematological Analyses on Mouse Blood. Curr Protoc Mouse Biol *3*, 101–119. https://doi.org/10.1002/9780470942390.MO130054.

Journal Pre-proof

Journal Pre-proof

FIGURE LEGENDS

Figure 1. *In vitro* validation of AASS knock-down by miR_AASS constructs. (A-B) Western blot and mRNA analysis of AASS in WT, miR_3 and miR_4 SH-SY5Y cell lines. (C-D) Western blot and mRNA analysis of AASS in WT, miR_3 and miR_4 NIH-3T3 cell lines. Quantification of AASS from different clones (n = 3). (E-F) Indirect measurement of AASS enzymatic activity, by luminescence assay determining the NADPH consumption in cell lysate. WT and miR_4 3T3 and SH-SY5Y cell lines, were cultured in the absence or presence of 10 mM lysine for 72h. NADPH consumption was directly proportional to AASS enzymatic activity. Data are expressed as the means ± SEM. Significance was assessed using a two-tailed Mann–Whitney test; *p < 0.05, **p < 0.01, ***p < 0.001.

Figure 2. Optimization of young adult administration of AAV-miR_AASS in *Gcdh-/-* mice to induce efficiently AASS knock-down. AAV-miR_AASS was injected at a dose (7.5×10^{12} vg/kg) into 1-month old mice using three procedures: intravenous administration via tail vein of AAV9 and AAV9P31 miR_AASS, and via cisterna magna. Analysis was performed 1-month post-treatment. (A) Schematic representation of AAV_miR_AASS. (B-C) Mature miR_AASS quantification in liver and striatum lysates (n=6-8). (D-E) Western blot analysis of AASS in liver and striatum lysates. Quantification of AASS from different individuals (n = 6). (F-G) GA, and 3-OH GA were measured in WT, *Gcdh-/-* saline, and *Gcdh-/-* AAV-miR_AASS treated mice in the liver and striatum (n=6-8). Data are expressed as the means ± SEM. Significance was assessed using a two-tailed Mann–Whitney test; *p < 0.05, **p < 0.01, ***p < 0.001.

Figure 3. Neonatal intravascular administration of AAV9_miR_AASS in *Gcdh-/-* mice induces efficiently AASS knock-down AASS in striatum. AAV9_miR_AASS was injected at two doses (7.5×10^{12} or 5×10^{13} vg/kg) into 1-2 days old mice via

temporal vein. Analysis were performed 1-month post-treatment. (A-B) Mature miR_AASS quantification in liver and striatum lysates (n=6-8). (C-D) Western blot analysis of AASS in liver and striatum lysates. Quantification of AASS from different individuals (n = 6). (E-F) GA, and 3-OH GA were measured in WT, *Gcdh-/-* saline, and *Gcdh-/-* AAV9_miR_AASS treated mice in the liver and striatum (n=6-8). Data are expressed as the means ± SEM. Significance was assessed using a two-tailed Mann–Whitney test; *p < 0.05, **p < 0.01, ***p < 0.001.

Figure 4. Rescue of weight loss and extended survival following neonatal intravascular administration of AAV9_miR_AASS in *Gcdh-/-* mice. AAV9_miR_AASS was injected at dose (5×10^{13} vg/kg) into 1-2 days old mice via temporal vein. (A) Scheme of the study. (B) Kaplan-Meier analysis of survival in *Gcdh-/-* saline and *Gcdh-/-* AAV9_miR_AASS mice on HLD after weaning (n=12-20). (C) Mouse body weight monitorization in WT, *Gcdh-/-* saline, and *Gcdh-/-* AAV9-miR_AASS mice on HLD after weaning. Measures were taken from weaning to 6-months (n=12-20).

Figure 5. Partial prevention of long-term metabolite accumulation in the liver induced by HLD following neonatal intravascular administration of AAV9_miR_AASS in *Gcdh-/-* mice. AAV9_miR_AASS was injected at dose (5×10^{13} vg/kg) into 1-2 days old mice via temporal vein. At weaning, animals were placed on HLD diet for 4 days or 5-months. Analysis was performed 1- and 6-month post-treatment. (A,C) Western blot analysis of AASS in liver lysates at 1- and 6-months. Quantification of AASS from different individuals (n = 6). (B,D) GA, and 3-OH GA were measured in WT, *Gcdh-/-* saline, and *Gcdh-/-* AAV9_miR_AASS treated mice in the liver at 1-and 6-months (n=6-8).

Figure 6. Slight prevention of liver morphological and functional alterations following neonatal intravascular administration of AAV9_miR_AASS in *Gcdh-/-*

mice. (A) Representative images of Hematoxylin & eosin (H&E)-stained liver sections in the indicated groups of mice at 1-and 6-months (scale bar: 50 μm). (B, C, D) Triglycerides, alkaline phosphatase activity and cholesterol levels were measured in serum of WT, *Gcdh-/-* saline, and *Gcdh-/-* AAV9_miR_AASS treated mice at 1- and 6-months fed on SD and HLD, respectively. Data are expressed as the means ± SEM. Significance was assessed using a two-tailed Mann–Whitney test; *p < 0.05, **p < 0.01.

Figure 7. Neonatal intravascular administration of AAV9_miR_AASS in *Gcdh-/-* mice prevents from HLD-induced metabolite accumulation in the striatum at 1-and 6-months post-treatment. AAV9_miR_AASS was injected at dose (5×10^{13} vg/kg) into 1-2 days old mice via temporal vein. At weaning, animals were placed on HLD diet for 4 days or 5-months. Analysis was performed 1- and 6-month post-treatment. (A,C) Western blot analysis of AASS in striatum lysates at 1-and 6-months. Quantification of AASS from different individuals (n = 6). (B,D) GA, and 3-OH GA were measured in WT, *Gcdh-/-* saline, and *Gcdh-/-* AAV9_miR_AASS treated mice in the striatum at 1- and 6-months (n=6-8). Data are expressed as the means ± SEM. Significance was assessed using a two-tailed Mann–Whitney test; *p < 0.05, **p < 0.01, ***p < 0.001.

Figure 8. Correction of striatal injury following neonatal intravascular administration of AAV9_miR_AASS in *Gcdh-/-* mice. Representative images of immunostaining of brain sections in the indicated groups of mice at 1- and 6-months. (A) Hematoxylin & eosin (H&E) staining shows progressive vacuolation in *Gcdh-/-* HLD mice (scale bar: 100 μm). (B) Immunohistochemistry with an specific antibody for the astrocyte marker GFAP (scale bar: 100 μm). (C) Immunostaining of brain sections from the same cohorts with myelin marker MBP (scale bar: 100 μm). Quantifications were performed on striatum regions with 1 section/mouse, digitalized with a ScanScope slide scanner, and analysed with QuPath 0.5.0 software (n=4). Results are presented as percentage of

893 vacuole area, GFAP-positive cells, or area of MBP staining. Data are expressed as the
894 means ± SEM. Significance was assessed using a two-tailed Mann–Whitney test; *p <
895 0.05, **p < 0.01, ***p < 0.001.
896

Journal Pre-proof

Journal Pre-proof

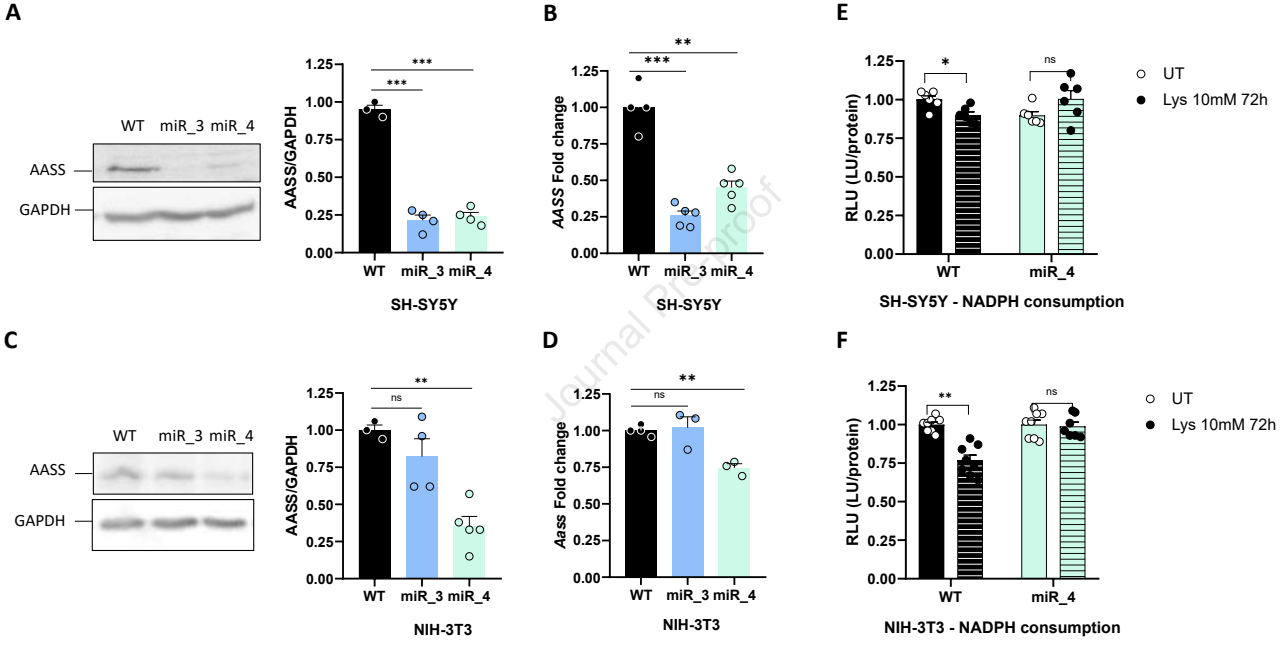

Journal Pre-proof

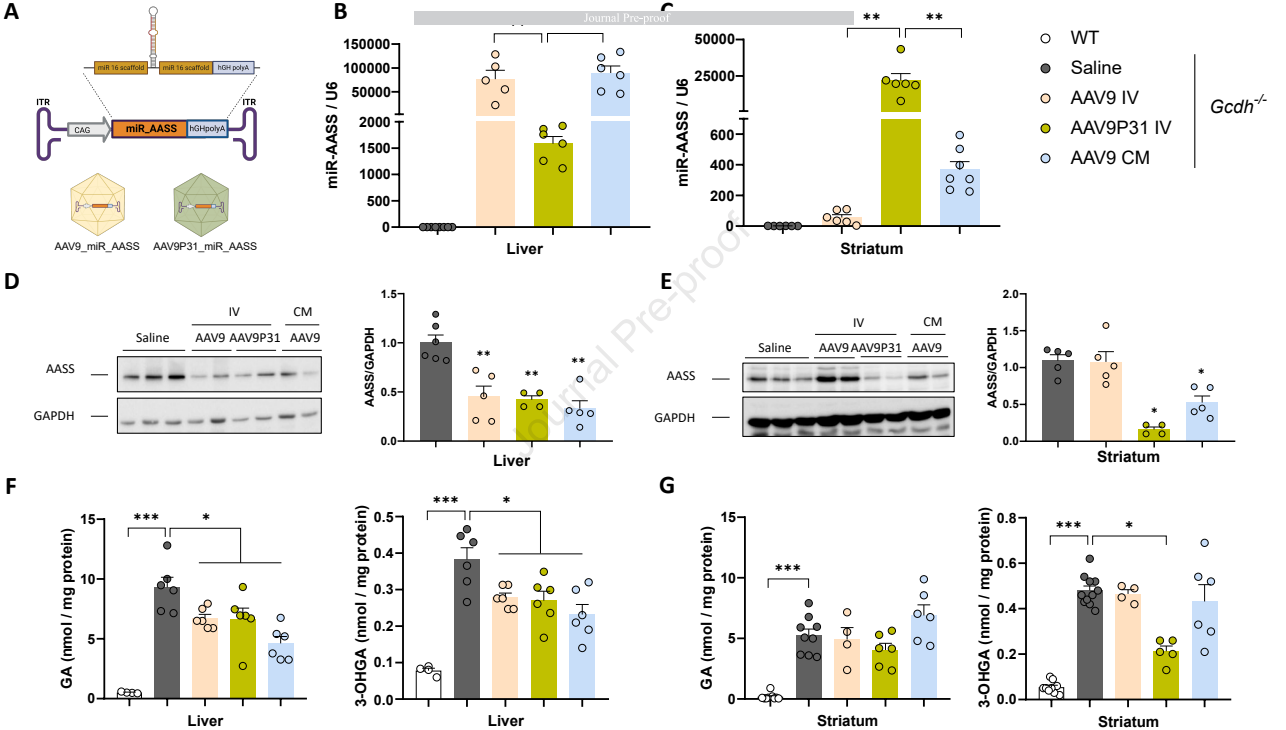

Journal Pre-proof

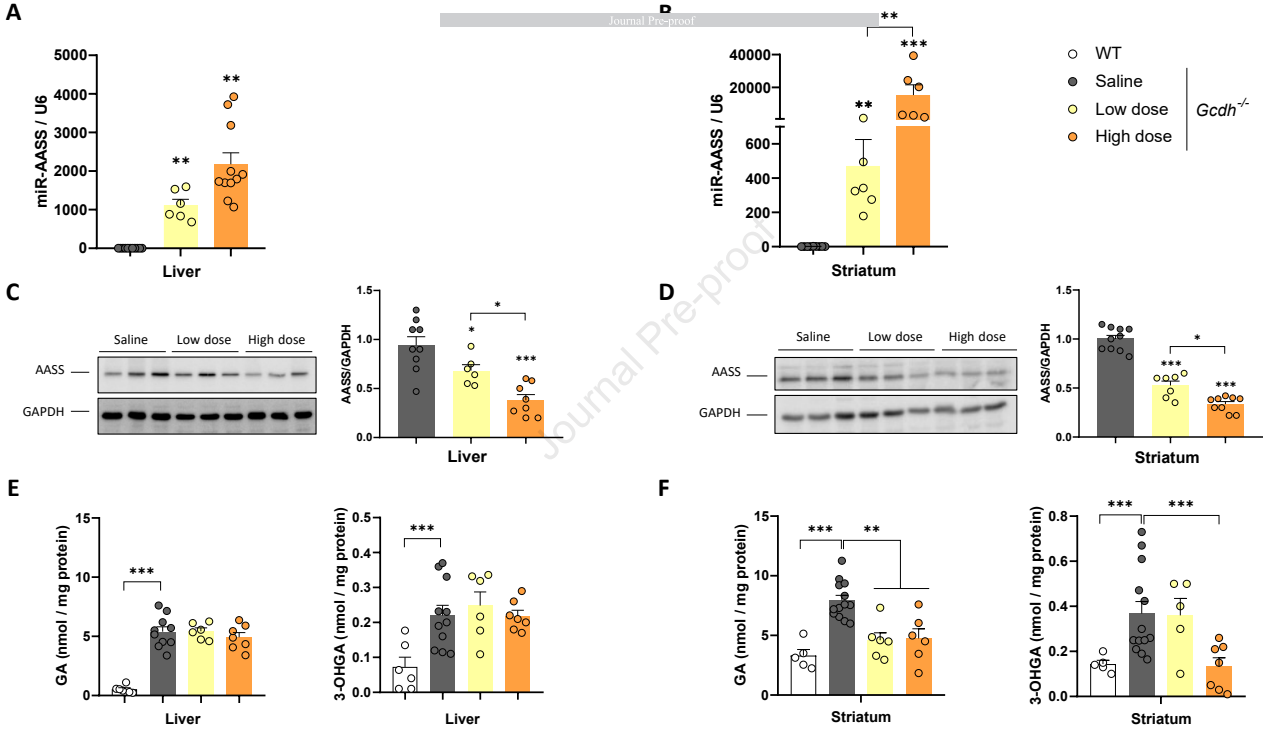

Journal Pre-proof

A

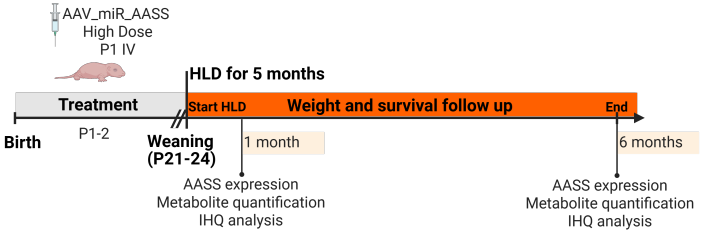

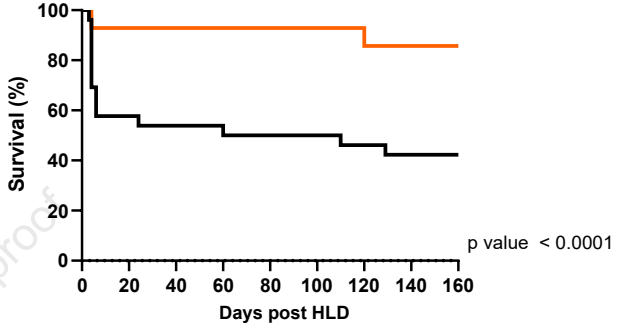

C

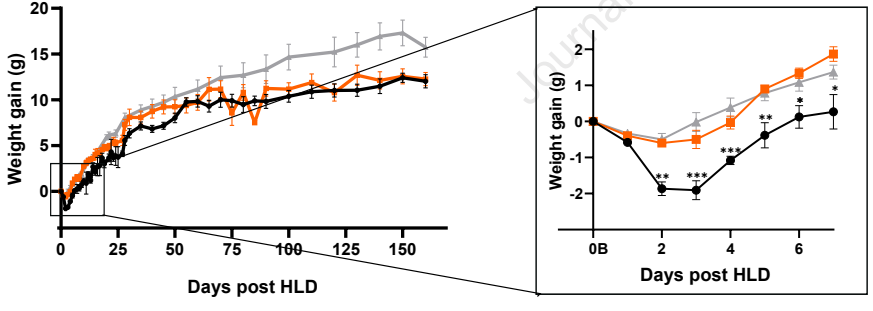

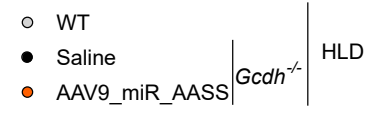

Journal Pre-proof

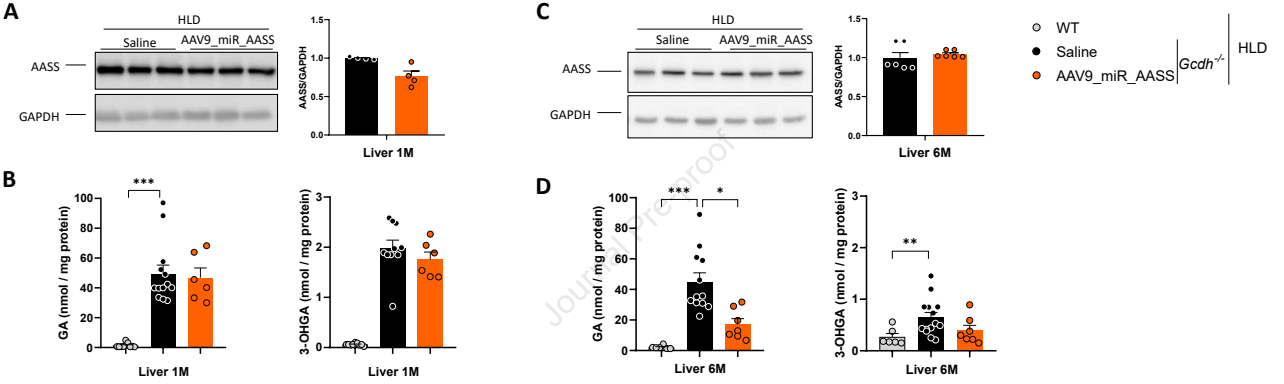

Journal Pre-proof

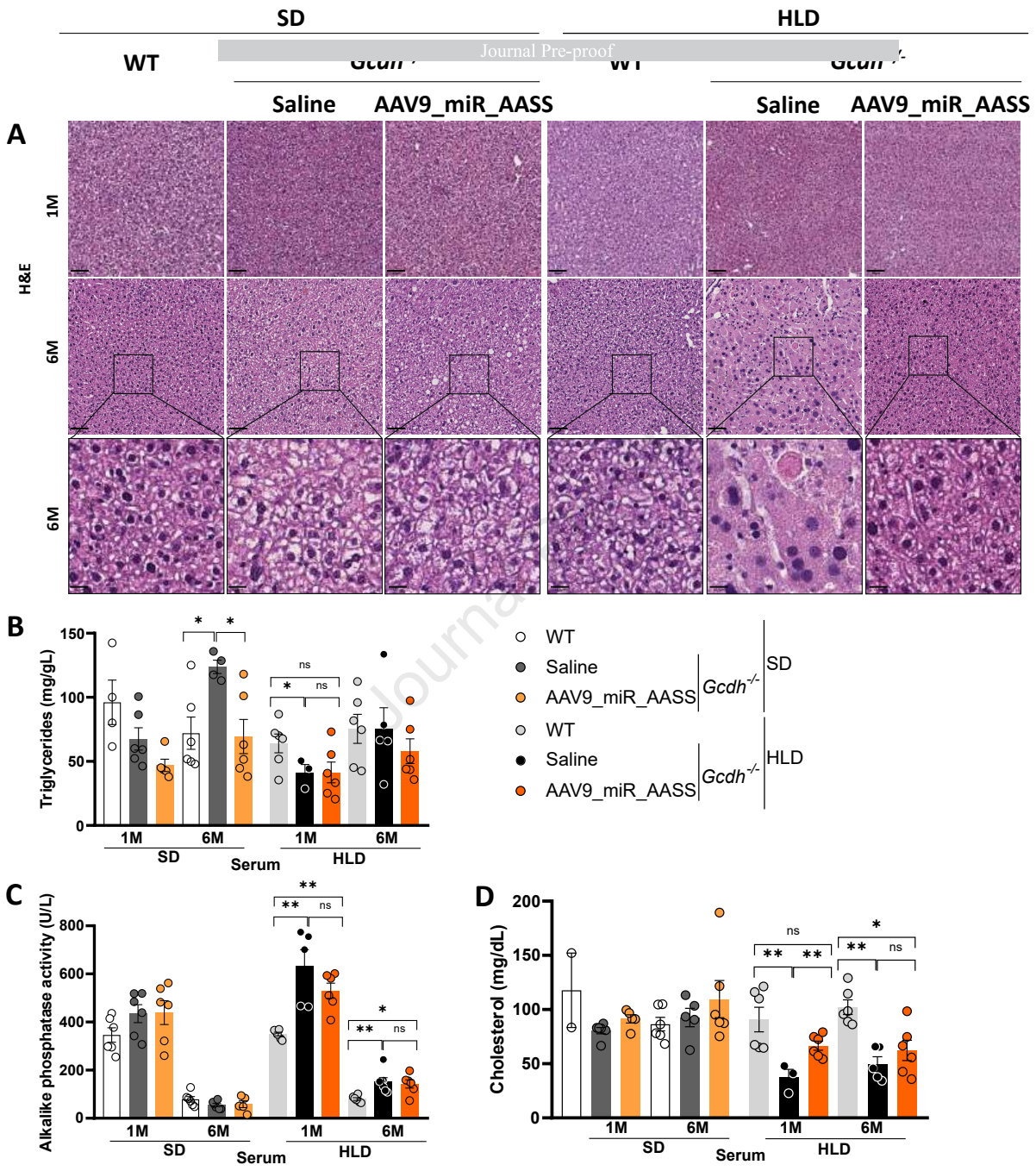

Journal Pre-proof

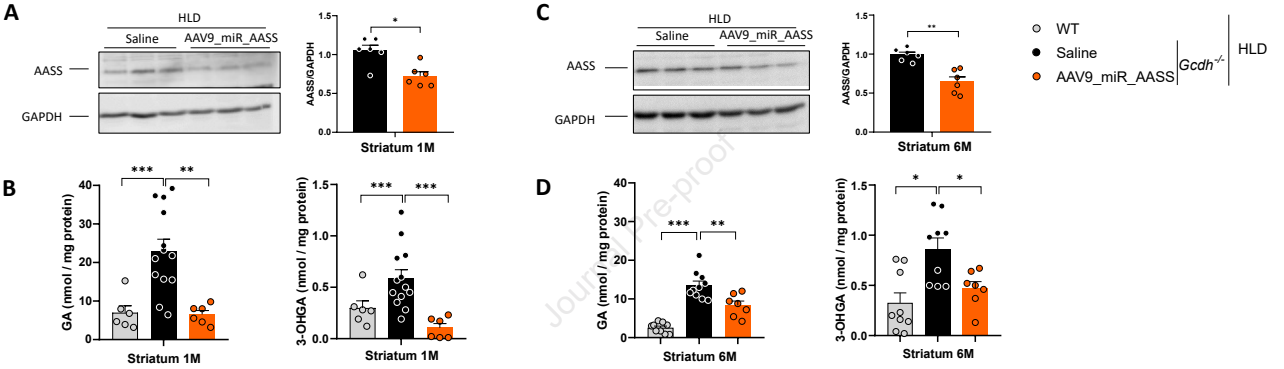

Journal Pre-proof

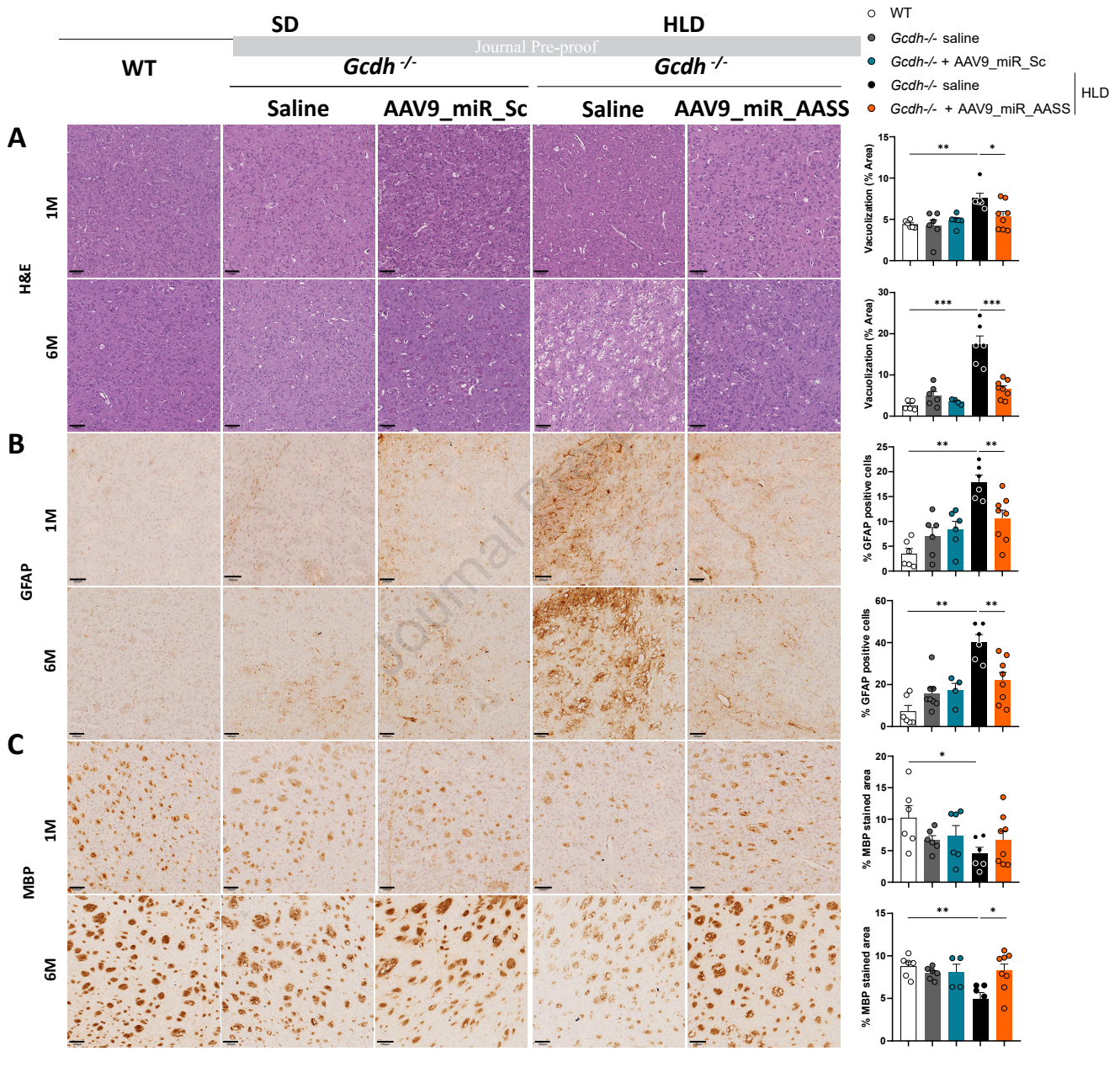

Journal Pre-proof

This study presents a substrate reduction therapy targeting the alpha-Aminoadipic Semialdehyde Synthase (AASS) enzyme, in the lysine catabolism as a therapeutic approach for glutaric aciduria type 1 (GA1). It develops an artificial microRNA recognizing AASS. Neonatal delivery of AAV9_miR_AASS in a GA1 mouse model ameliorates their phenotype and expands survival.

Journal Pre-proof